JPPIPA 11(9) (2025)

Jurnal Penelitian Pendidikan IPA

http://jppipa.unram.ac.id/index.php/jppipa/index

Fault Identification Using Satellite Imagery, Gravity, and Seismicity Data on Lombok Island

Muhammad Aryanto[1,2*], Ira Mutiara Anjasmara[1], Putra Maulida[1]

[1] Departemen of Geomatics Engineering, Faculty of Planning, and Earth Engineering, Institut Teknologi Sepuluh Nopember, Surabaya ITS Sukolilo Campus, Surabaya, Indonesia.
[2] Indonesia Agency for Meteorology, Climatology and Geophysics (BMKG), Jakarta, Indonesia.

Received: July 14, 2025
Revised: August 16, 2025
Accepted: September 25, 2025
Published: September 30, 2025

Corresponding Author:
Muhammad Aryanto
muhammad.aryanto@bmkg.go.id

DOI: 10.29303/jppipa.v11i9.12533

Abstract: Lombok Island has a high level of earthquake vulnerability due to local tectonic activities. Although most earthquakes on land have small magnitudes (M < 5), their proximity to settlements has the potential to cause significant impacts. This study aims to identify the potential for active faults using a multi-data approach, specifically utilizing gravity anomaly data from GGMplus. In addition, Sentinel-1 data is used for surface lineament extraction and DEMNAS for topography. Analysis of gravity data utilizing GGMPlus reveals that the Batujahe Fault exhibits thrust faulting characteristics, whereas the South Lombok Fault displays normal faulting behavior. Automated lineament extraction yielded a total of 54 surface structural lineaments within the study area, spanning a cumulative length of 478 km. These results provide a shorter fault length than the existing fault map. Statistical analysis of the extracted lineaments revealed three dominant trends: N-S, NE-SW, and NW-SE, with the N-S trend being the most predominant. Notably, these findings diverge from prior studies, which classified the Batujahe Fault as a strike-slip fault and the South Lombok Fault as a thrust fault, underscoring the complexities of fault dynamics in the region, however derivative methods fail to detect the Alas Strait strike-slip fault.

Keywords: Fault; GGMplus; Lombok; Mitigation; Sentinel-1

Introduction

Generally, earthquakes in the northern mainland of Lombok are caused by the Flores Back Arc thrust, but there are several earthquakes that have different movement patterns and there are also shallow earthquakes that occur in the southern part of Lombok Island. This indicates the presence of local fault activity on the mainland of Lombok Island. In a period of 56 years (1963 – 2018), it was recorded that the Flores Back Arc Thrust system north of Bali to Lombok triggered seven significant and damaging earthquakes (Mw > 6.0) (Gunawan et al., 2020). On the other hand, on March 17, 2019, another significant earthquake was reported to have caused damage. The earthquakes with magnitudes Mw 5.4 and Mw 5.1 that occurred within minutes were reported to have caused damage to buildings in the East Lombok area and were felt as far away as Bali. However, interestingly, unlike the characteristics of the Flores Back Arc Thrust earthquake, based on the catalog from The Global Centroid-Moment-Tensor (CMT) Project, both earthquakes had a normal fault type source mechanism (Dziewonski et al., 1981; Ekström et al., 2012).

According to the National Earthquake Study Center (Irsyam et al., 2017), the Lombok region features several faults, including the Flores Back Arc Thrust Fault, Lombok Strait Strike-slip Fault, and Sumbawa Strait Strike-slip Fault, primarily located offshore. However, no active faults are mentioned for the mainland area of Lombok Island. In contrast, based on active fault Indonesia map (Soehaimi et al., 2021) identifies three faults on Lombok Island there are Batujahe Strike-slip

How to Cite:
Aryanto, M., Anjasmara, I. M., & Maulida, P. (2025). Fault Identification Using Satellite Imagery, Gravity, and Seismicity Data on Lombok Island. *Jurnal Penelitian Pendidikan IPA*, *11*(9), 805–812. https://doi.org/10.29303/jppipa.v11i9.12533

Fault, South Lombok Thrust Fault, and Alas Strait Strike Slip Fault. Based on seismicity and the existence of faults that currently exist, there are differences where many shallow earthquakes do not have corresponding faults. This is because there is still a lack of research on faults in the Lombok area and it is still very possible for new faults that have not been identified.

Advanced remote sensing techniques, particularly radar and gravity datasets, provide powerful tools for studying such challenging terrains and wide area. In addition, as supporting data from seismicity, since the end of the 2010s, BMKG has increased the sensor network so as to increase the completeness of the earthquake catalog in the Lombok region in earthquake analysis. This can be seen spatially from the decrease in the magnitude completeness (Mc) value in areas with the addition of new sensors and temporally from the decrease in the gradient of the Mc value over time (Pratama et al., 2021).

Mapping of fault areas on the mainland of Lombok using remote sensing methods is needed to identify faults on Lombok Island. Determination of the position and type of fault is then validated with seismicity data and geological maps. This processing will produce the location, type, and model of the subsurface structure of local faults in Lombok. The results of this study are expected to be used as an update of active faults on land and earthquake hazard maps on Lombok Island.

Method

The data used in this study were retrieved from the earthquake catalogues of the International Seismological Centre Engdahl-van der Hilst-Buland (ISC-EHB) (Engdahl et al., 2020) dan The Agency for Meteorology, Climatology, and Geophysics of the Republic of Indonesia (BMKG). Analyzing data from different sources, such as satellite imagery, high-resolution DEMs, and geological surveys, to enhance the understanding of fault geometry and activity (Ha et al., 2025).

This study utilizes pre-processed Sentinel-1 C-band dual-polarization (VV and VH) SAR data accessed via Google Earth Engine (GEE), a cloud-based geospatial analysis platform. Within GEE, the standard preprocessing steps include thermal noise removal, radiometric calibration, and terrain correction. Given the inherent salt-and-pepper noise characteristic of SAR data, speckle filtering is a critical preprocessing step. To address this, a time-series of Sentinel-1 Ground Range Detected (GRD) SAR data acquired over the study area in 2018 was employed to perform multi-temporal speckle filtering. This approach effectively reduces speckle noise while preserving spatial resolution and essential information content (Ghosh et al., 2021). The filtering process involves computing the mean backscatter value for each pixel across multiple temporal acquisitions. Subsequently, all Sentinel-1 SAR datasets were co-registered and resampled to a spatial resolution of 25 meters.

To minimize the misclassification of high-contrast land cover features—such as water bodies, agricultural fields, and urban areas—as geological lineaments by the LINE module, slope data derived from the Shuttle Radar Topography Mission (SRTM) Digital Elevation Model (DEM) was used to mask flat terrain regions in the SAR imagery. Following this, automatic lineament extraction was conducted using the PCI Geomatica software. The LINE tool, specifically designed for radar imagery, was employed to extract linear features and represent them in polyline vector format. The extraction process consists of two main stages: contour detection and line detection. Contour detection is performed using the RADI (filter radius) parameter via the Canny edge detection algorithm, which effectively delineates feature boundaries within the SAR images.

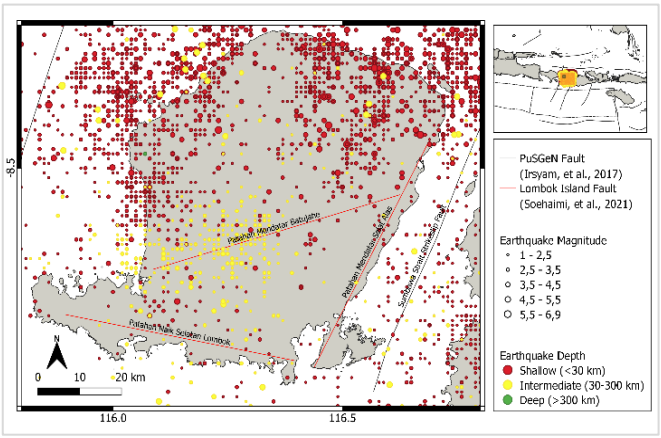

Figure 1. Seismicity of Lombok Island (data from ISC-EHB and BMKG)

Geologically, Lombok Island is composed of the youngest rocks in the Holocene era to the oldest in the Tertiary era (Mangga et al., 1994). Rocks with Holocene and Pleistocene (Quaternary) ages dominate the central and southern parts of Lombok Island which are composed of surface deposits, sedimentary rocks and volcanic rocks, while Tertiary age rocks dominate the southern coast of Lombok Island.

The gravity data used in this study are Free-Air Anomaly (FAA) data with a spatial resolution of approximately 200 meters, obtained from https://ddfe.curtin.edu.au/gravitymodels/GGMplus/data/. The model combines satellite-derived gravity data from GRACE and GOCE, the EGM2008 global geopotential model, and high-resolution topographic data from SRTM, as described by Hirt et al. (2013).

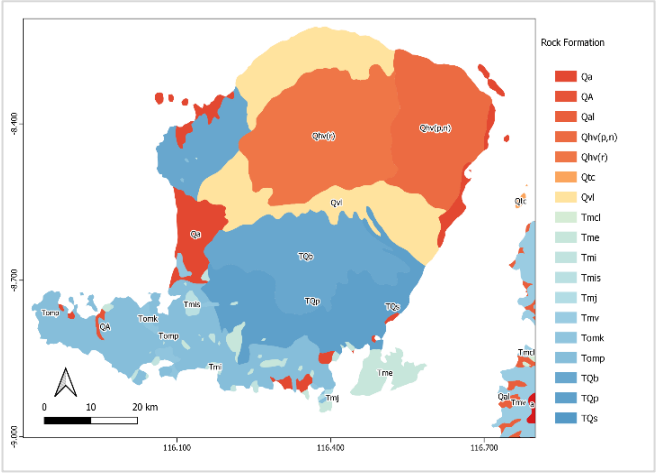

Figure 2. Geological conditions of Lombok Island (reprocessed from ESDM (2024) and Soehaimi et al. (2021))

The Free-Air Anomaly data were then corrected using a simple Bouguer correction, assuming an average crustal density of 2.67 g/cm³, resulting in a Simple Bouguer Anomaly. To further account for complex surface relief, a terrain correction was applied, yielding the Complete Bouguer Anomaly (CBA), following standard gravity data processing procedures (Telford et al., 1990).

Complete Bouguer Anomaly (CBA) data were analyzed to separate the regional anomaly components and residual anomalies. Separation was done by differentiating high frequencies for shallow depths and low frequencies for deeper structures. Spectrum analysis with Fourier transform of the relationship between amplitude (A) and wave (k) (Blakely, 1996).

$$A = (z - z_o) \vee k \vee \quad (1)$$

The depth of the density discontinuity field will be proportional to the slope of the spectrum graph. The window width estimation equation is as follows with the window width (n), cut-off wavenumber (kc), and spatial distance (ΔS).

$$n = 2\,\pi/(\Delta S.\, kc) \quad (2)$$

The moving average filter is good enough to remove regional effects originating from deeper sources, leaving residual anomalies representing shallow geological structures (Blakely, 1996). This method produces regional anomalies that represent low-frequency anomalies for deep structures. Subtracting bouguer anomalies (CBA) from regional anomalies will produce high-frequency residual anomalies for shallow structures.

The residual anomaly is then subjected to the First Horizontal Derivative (FHD) to display lateral changes in gravity values, which describe geological boundaries such as faults or differences in rock structure (Hinze et al., 2013). According to Cordell et al. (1982), it is formulated as follows:

$$FHD = \sqrt{\left(\frac{\partial g}{\partial x}\right)^2 + \left(\frac{\partial g}{\partial y}\right)^2} \quad (3)$$

with $\left(\frac{\partial g}{\partial x}\right)$ and $\left(\frac{\partial g}{\partial y}\right)$ the first derivative of the anomaly in the x and y directions of the FHD has maximum and minimum values that interpret differences in geological structures or boundaries.

Next, a Second Vertical Derivative (SVD) filter is performed based on the Elkins approach to strengthen the indication of vertically adjacent structures, thus assisting in the interpretation of direction and geometry such as faults (Elkins, 1951; Sarkowi, 2010). The Laplace equation for anomalies is as follows (Telford et al., 1990).

$$\nabla^2 \Delta g = 0 atau \frac{\partial^2 \Delta g}{\partial x^2} + \frac{\partial^2 \Delta g}{\partial y^2} + \frac{\partial^2 \Delta g}{\partial z^2} = 0 \quad (4)$$

$$\frac{\partial^2 \Delta g}{\partial z^2} = -\left(\frac{\partial^2 \Delta g}{\partial x^2} + \frac{\partial^2 \Delta g}{\partial y^2}\right) \quad (5)$$

with Δg is gravity anomaly value, $\frac{\partial^2 \Delta g}{\partial z^2}$ for the second derivative value of the vertical direction gravity field. The SVD filter has an amplitude response as follows (Elkins, 1951).

0,00	-0,0833	0,00	-0,0833	0,00
-0,0833	-0,0667	-0,0334	-0,0667	-0,0833
0,00	-0,0334	1,0668	-0,0334	0,00
-0,0833	-0,0667	-0,0334	-0,0667	-0,0833
0,00	-0,0833	0,00	-0,0833	0,00

Figure 3. SVD Filter amplitude response

The difference in structure can be interpreted if the SVD is 0. The type of fault can be seen from the (Telford et al., 1990) resulting SVD value. SVD is used to determine the type of fault with the following provisions (Sarkowi, 2010).

$$\frac{\partial^2(\Delta g)}{\partial z^2} \vee \quad maks > \frac{\partial^2(\Delta g)}{\partial z^2} \vee \quad min, \text{ for normal fault} \quad (6)$$

$$\frac{\partial^2(\Delta g)}{\partial z^2} \vee \quad maks < \frac{\partial^2(\Delta g)}{\partial z^2} \vee \quad min, \text{ for thrust fault} \quad (7)$$

$$\frac{\partial^2(\Delta g)}{\partial z^2} \vee \quad maks = \frac{\partial^2(\Delta g)}{\partial z^2} \vee \quad min, \text{ for strikeslip fault} \quad (8)$$

Then FHD and SVD were cut for interpretation of subsurface structure.

Result and Discussion

During the period 1963-2018, the total seismic energy released of the Flores Back Arc Thrust zone of the Lombok segment was not less than 1.50 x 1015 Joules or equivalent to Mw 7.3 (Gunawan et al., 2020), while based on Irsyam et al. (2017) it has the potential for an earthquake with a maximum magnitude of Mw 7.4 or equivalent to 2.01 x 1015 Joules. Most of the earthquakes on the Lombok mainland that are indicated to be caused by local faults are possibly triggered by the energy release activity of a series of large earthquakes by the Flores Back Arc Thrust system in 2018.

The Sentinel-1 SAR datasets processed with the LINE module were evaluated to determine how SAR sensor parameters like frequency, polarization, and look direction impact the automatic extraction of geological lineaments. Both qualitative and quantitative analyses were conducted on the data derived from each parameter, and a detailed comparison of these factors is presented in the following sections.

The SAR dataset acquired at C-band frequency in both like and cross polarization are considered for this analysis. In order to compensate for the effect of look-direction, SAR dataset acquired at nearly the same look-direction were taken into consideration. The C-band like-polarization SAR data acquired in ascending and descending passes are used to analysis the influence of sensor look-direction for lineament extraction. In addition to this qualitative analysis, quantitative para meters such as, number and length of lineaments in each direction are measured for both ascending and descending passes.

Integrating multi-look direction C-band SAR data enhances the reliability of lineament mapping in the study area. The process focused on lineaments oriented between 270°–360° from ascending and 0°–90° from descending tracks, due to their near-perpendicular alignment with the SAR sensor's look direction during data acquisition.

In the first stage of automatic lineament extraction, a radius filter was performed. Based on terrain correction in pre-processing, a pixel spacing of 25 m was obtained. By using RADI = 5, the calculated pixel distance must be longer than 125 m. Based on this value, the local maxima were determined, so that pixels that are not included in the edge pixel value of 5 are removed. The results leave only a thin line feature. Finally, the image pixel value that has a gradient value beyond the maximum value was substituted with a value of 0.

The second stage, thresholding was used to create a binary image. Each image pixel represents an edge element, the threshold value for each pixel was determined based on the GTHR parameter. The GTHR value affects the number of line segments resulting from the extraction process. All input data passed a re-stretching process to become an 8-bit value, so that the GTHR parameter is in the value range 0-255. From the results of the input data used through a series of experiments using trial and error, the value of GTHR = 50 was obtained. This value is appropriate because if we use a low GTHR value there are too many line features that are generated and close to each other (visually) and vice versa.

The third stage, curve extraction is to extract curves from binary images which consist of several extraction sub-stages. The line thinning stage has a thinning algorithm to produce a per-pixel curve frame. The extraction stage for a series of pixels as a curve removes values smaller than the parameter LTHR = 30 pixels or 750 m. The pixel-based raster data extracted results into vector data by matching line segments so that the result is a segment that has close proximity to the extracted pixel pattern based on the maximum value of the fitting error determined by the FTHR. The FTHR value indicates the maximum tolerance for the distance between a curve (pixel-based) and the segment pattern formed. Lower values provide better fitting, but also shorter segments in the polyline. The FTHR = 4 setting used higher a pixel conforms to the default of the LINE Module. Furthermore, the algorithm connects the line segments are based on ATHR. The two ends of the segments of the two polylines are opposite each other in the same direction with an angle difference of less than ATHR = 20 degrees. If the line is greater than 20 degrees it will make the fault look very crooked.

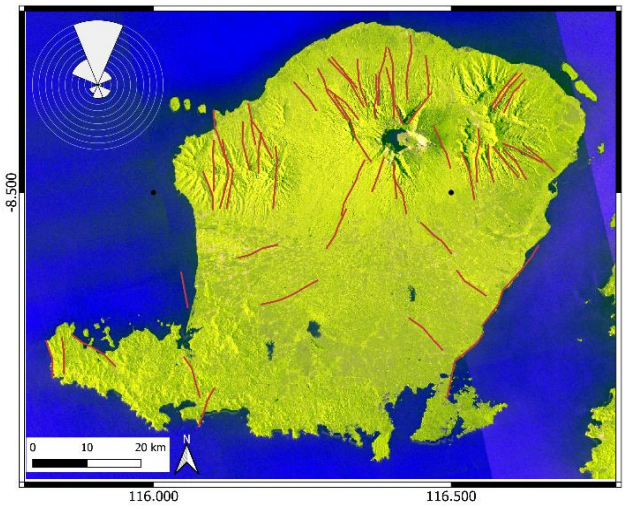

Figure 4. Lineament extraction from Sentinel-1 using LINE module

A total of 54 surface structural lineaments were extracted automatically in the study area, with a total lineament length of 478 km. The automatically extracted

lineaments display three major trends (N-S, NE-SW, and NW-SE), with the prevalent being the N-S. The length of the smallest lineament extracted in the area was 4 km, while the largest lineament was 18 km in length with the mean length was 8.7 km.

The clustering of high lineament density anomalies in the northern and northeastern study area suggests a strong link between structural features and geothermal activity. This could be attributed to the influence of igneous intrusions and recent tectonism. Conversely, in the southern region, closer to the coastal plain and away from thermal springs, the correlation between surface and subsurface lineament densities weakens. For the South Lombok region, the orientation of the lineaments in this area is similar to Jundiy et al. (2023) which has NNW-SSE lineament trends using DEM data. In addition, the similarity of the lineament orientations is also in accordance with Agung et. al. (2021) the general direction in Sembalun Area is NE-SW.

This study underscores the significance of localized minor folds, faults, and stress fields within a highly tectonically active region. The structural anomalies identified in the area provide critical insights into their relationship with broader regional structural patterns. Continued research in this domain will enhance our understanding of the spatial distribution of geohazards such as landslides and earthquakes, and will also contribute to the detection of concealed or buried fault systems.

Complete Bouguer Anomaly (CBA) (Figure 1) describes the distribution of gravity anomaly values as shown in the image above with the range of values is from 40 to 190 mGal. High CBA values describe rocks with higher densities in the subsurface structure which it generally comes from the magmatic activity of Mount Rinjani. North and East Lombok are usually dominated by young volcanic deposits from Mount Rinjani. While Central and South Lombok are older volcanic deposits.

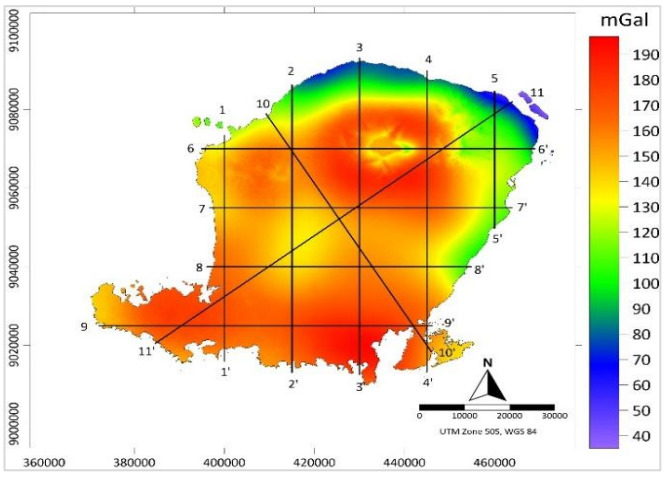

Figure 5. Complete bouguer anomaly (CBA) of Lombok Island with slicing

Ten slices were performed for spectrum analysis consisting of 5 north-south slices, 4 west-east slices, 1 northwest-southeast, and 1 northeast-southwest. The following (Figure 2) are the results of the spectrum analysis performed to separate regional anomalies and residual anomalies.

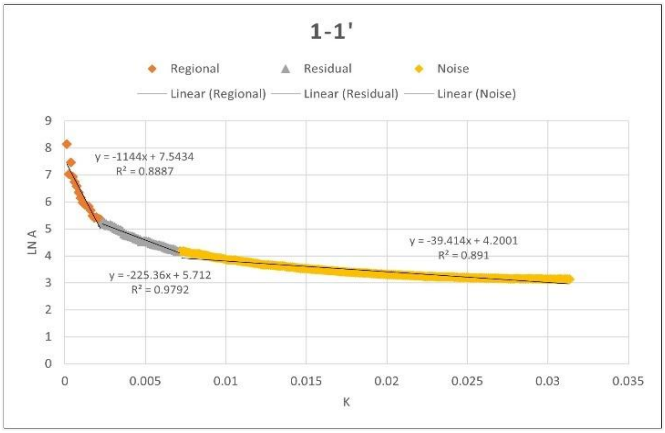

Figure 6. Spectrum analysis for section 1-1′

Figure 2 describes a spectrum analysis for sample section 1-1′ with the x-axis as wavenumber and the y-axis as ln A. The sharp decreasing trend in the regional section indicates a signal with low frequency or high wavelength with a non-steep slope interpreting regional anomalies in deep structures. The residual section has a steep slope of high frequency or shorter wavelength interpreting residual anomalies for shallow depth structures. While the noise section has a gentle slope with very high frequencies that can indicate measurement noise or surface structure effects.

The following is a summary table of the results of 10 sections performed to separate regional and residual anomalies.

Table 1. Spectrum Analysis Results

Slices	Regional	Residual	K Cut off
1-1'	1144.0	225.36	$1.99x10^{-3}$
2-2'	2145.1	316.22	$1.06 x10^{-3}$
3-3'	2655.0	306.51	$9.80 x10^{-4}$
4-4'	2482.9	317.51	$1.00 x10^{-3}$
5-5'	1239.5	158.51	$2.01 x10^{-3}$
6-6'	1265.8	205.33	$2.24 x10^{-3}$
7-7'	2602.5	271.08	$1.16 x10^{-3}$
8-8'	1061.0	217.48	$2.10 x10^{-4}$
9-9'	1045.3	213.25	$2.16 x10^{-3}$
10-10'	1298.1	240.93	$1.64 x10^{-3}$
11-11'	1608.6	244.36	$1.53 x10^{-3}$

In general, the results of the spectrum analysis describe the position of the geological structure. From the table above, the highest regional value in slices 3-3 'and 4-4' with values 2655 and 2482.9 indicates a deeper and larger structure, in accordance with the high

residual value affected by the large structure in the region. The lambda value which is also high or low frequency describes the dominant deep structure from the position of slices 3-3 'and 4-4' located close to Mount Rinjani.

The N value is the wavelength to the data spacing. In this study, the data spacing is 100 m and the N value varies between 28-64. The higher the N value, the more dominant the regional anomaly is in proportion to the large wavelength and low frequency. For uniformity and consistency in determining the N value, the value that often appears ranges from 28-31, so the N value = 29 is used.

After the anomaly separation is done using the moving average method, regional anomalies are obtained. To obtain residual anomalies (Figure 2), CBA are subtracted from regional anomalies. In general, high anomalies are in the northern region which is the Mount Rinjani zone. In the central part, it shows a wide negative anomaly depicting a sedimentary basin due to volcanic activity. The structure on Lombok Island is quite complex due to volcanic and tectonic activity.

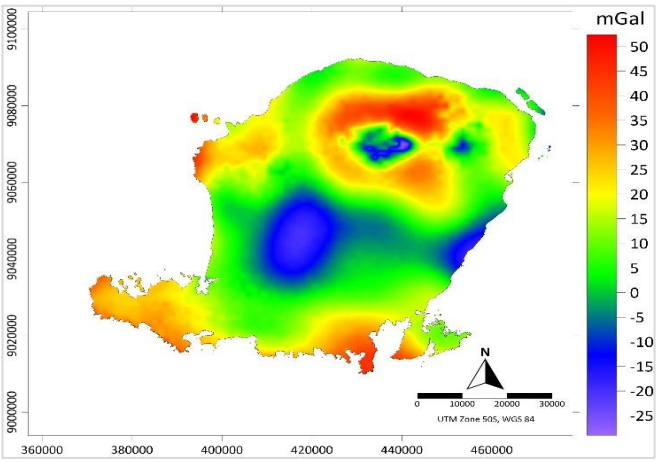

Figure 7. Residual anomaly of Lombok Island

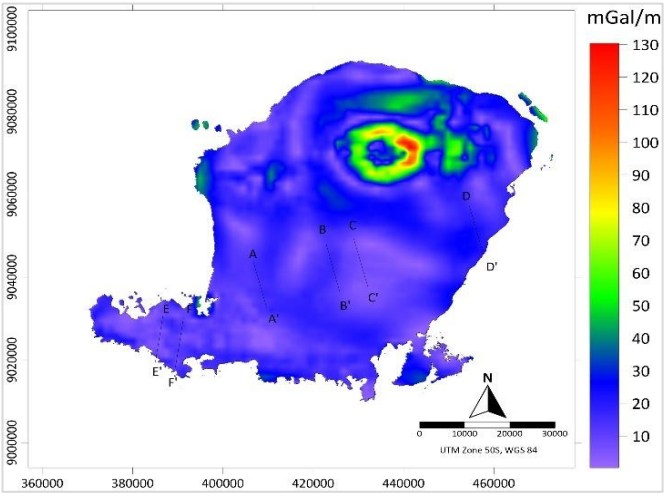

Figure 8. First horizontal derivative

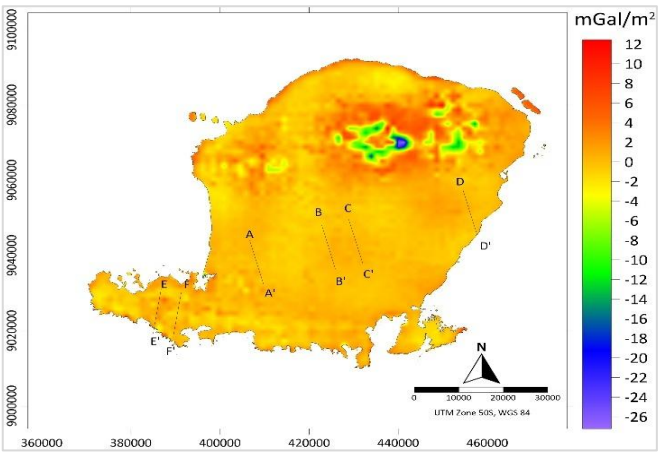

Figure 9. First horizontal derivative (FHD) and second vertical derivative (SVD) of Lombok Island

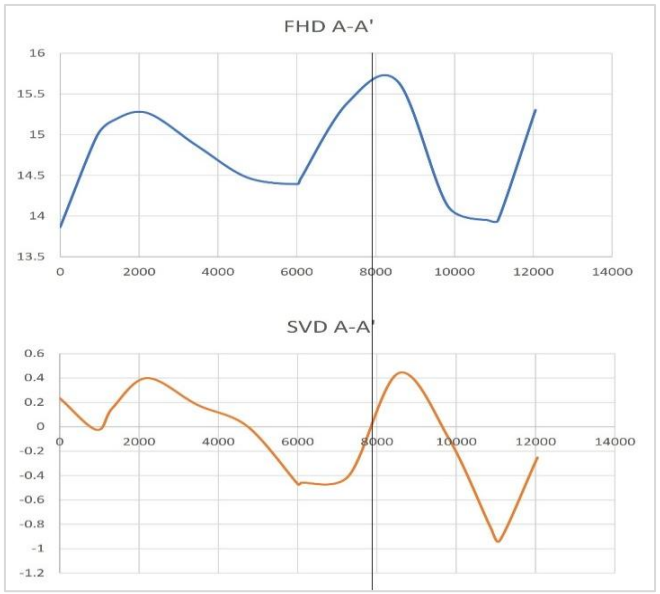

Figure 10. Slicing FHD and SVD of A-A' line

The residual anomalies obtained are then filtered using the First Horizontal Derivative (FHD) and Second Vertical Derivative (SVD) (Figure 5) methods to identify subsurface structural features, especially indications of faults and to confirm existing faults.

Based on gravity data analysis, FHD and SVD methods fail to detect the strike-slip fault in the Alas Strait. Notably, our results contrast with previous research, which characterized the Batujahe Fault as strike-slip and the South Lombok Fault as thrust, emphasizing the intricate nature of fault dynamics and the importance of ongoing investigation to further elucidate the region's tectonic framework.

Conclusion

An in-depth analysis of gravity data utilizing the GGMPlus model reveals distinct faulting mechanisms

for the Batujahe and South Lombok Faults, providing valuable insights into the tectonic framework of the region. Specifically, the Batujahe Fault exhibits characteristic thrust faulting behavior, whereas the South Lombok Fault displays normal faulting behavior, highlighting the complex interplay of tectonic forces in the area. Furthermore, automated lineament extraction yielded a total of 54 surface structural lineaments within the study area, spanning a cumulative length of 478 km. Notably, these results indicate a shorter fault length compared to the existing fault map, potentially suggesting a more nuanced understanding of fault distribution and geometry. Statistical analysis of the extracted lineaments revealed three dominant trends: N-S, NE-SW, and NW-SE, with the N-S trend being the most predominant, implying a strong structural control on the regional geology. Interestingly, these findings diverge from prior studies, which classified the Batujahe Fault as a strike-slip fault and the South Lombok Fault as a thrust fault, underscoring the complexities of fault dynamics in the region and highlighting the need for continued research to refine our understanding of the local tectonic setting.

Acknowledgments
The authors gratefully acknowledge the following organizations for providing essential data and resources: European Space Agency (Sentinel-1 SAR data), Curtin University (GGMPlus data), ISC-EHB and Indonesian Agency for Meteorology, Climatology, and Geophysics (BMKG) (earthquake catalog), Geological Agency of Indonesia (Lombok geological map), Indonesian Geospatial Information Agency (BIG) (DEMNAS data), and Google LLC (Google Earth and Google Earth Engine Cloud Platform).

Author Contributions
Conceptualization, M. A. and I. M. A.; methodology, M. A.; software, M. A.; validationM. A., I. M. A. P. M.; formal analysis, Muhammad Aryanto; investigation, M. A.; resources, M. A.; data curation, M. A.; writing—original draft preparation, M. A.; writing—review and editing, I. M. A. and P. M.; visualization, M. A.; supervision, I. M. A.; project administrationI. M. A.; funding acquisition, none. All authors have read and agreed to the published version of the manuscript."

Funding
This research received no external funding

Conflicts of Interest
The authors declare no conflict of interest.

References

Agung, Y. Z., Haryanto, A. D., Hardiyono, A., Setiawan, D. I., & Suleman, W. A. (2021). High permeability zone on geothermal manifestations using fault fracture density in Sembalun Area, Lombok. *Journal of Geological Sciences and Applied Geology, 5*(2). https://doi.org/10.24198/gsag.v5i2.34937

Al Jundiy, M. H. (2023). Aplikasi Metode Lineament Density Analysis Untuk Pemetaan Potensi Zona Mineralisasi: Studi Kasus Daerah Sekotong, Lombok Selatan. *Jurnal Teknik Geologi: Jurnal Ilmu Pengetahuan dan Teknologi, 6*(1), 20-26. Retrieved from https://ocs.unmul.ac.id/index.php/TG/article/view/12201

Blakely, R. J. (1996). *Potential Theory in Gravity and Magnetic Applications*. Cambridge University Press.

Bunaga, I. G. K. S., Rosid, M. S., & Anggono, T. (2022). Existence of Faults that Cause Earthquakes on Lombok Island: A Critical Literature Review. *Jurnal Penelitian Pendidikan IPA*, *8*(6), 2827–2832. https://doi.org/10.29303/jppipa.v8i6.2346

Dziewonski, A. M., Chou, T.-A., & Woodhouse, J. H. (1981). Determination of earthquake source parameters from waveform data for studies of global and regional seismicity. *Journal of Geophysical Research: Solid Earth*, 86(B4), 2825–2852. https://doi.org/10.1029/JB086iB04p02825

Ekström, G., Nettles, M., & Dziewoński, A. M. (2012). The global CMT project 2004–2010: Centroid-moment tensors for 13,017 earthquakes. *Physics of the Earth and Planetary Interiors*, *200–201*, 1–9. https://doi.org/10.1016/J.PEPI.2012.04.002

Elkins, T. A. (1951). The second derivative method of gravity interpretation. *Geophysics*, *16*(1), 29–50. https://doi.org/10.1190/1.1437648

Engdahl, E. R., di Giacomo, D., Sakarya, B., Gkarlaouni, C. G., Harris, J., & Storchak, D. A. (2020). ISC-EHB 1964–2016, an Improved Data Set for Studies of Earth Structure and Global Seismicity. *Earth and Space Science*, *7*(1). https://doi.org/10.1029/2019EA000897

Ghosh, S., Sivasankar, T., & Anand, G. (2021). Performance evaluation of multi-parametric synthetic aperture radar data for geological lineament extraction. *International Journal of Remote Sensing*, *42*(7), 2574–2593. https://doi.org/10.1080/01431161.2020.1856963

Gunawan, T., Damayanti, A. P. R., & Gunawan, M. T. (2020). Studi Karakteristik Gempabumi Signifikan Mw > 6.0 Akibat Aktivitas Sistem Busur Belakang Segmen Bali Lombok Menggunakan Analisis Energi Kumulatif dan Periode Ulang. *Jurnal Meteorologi dan Geofisika*, *21*(1), 29–35. https://doi.org/10.31172/jmg.v21i1.625

Ha, S., Kang, H. C., Lee, S., Seong, Y. B., Choi, J. H., Kim, S. J., & Son, M. (2025). Quaternary surface ruptures of the inherited mature Yangsan Fault: implications for intraplate earthquakes in

southeastern Korea. *Solid Earth*, *16*(2), 197–231. https://doi.org/10.5194/se-16-197-2025

Hinze, W. J., von Frese, R. R. B., & Saad, A. H. (2013). *Gravity and Magnetic Exploration: Principles, Practices, and Applications*. Cambridge University Press. https://doi.org/10.1017/CBO9780511843129

Hirt, C., Claessens, S., Fecher, T., Kuhn, M., Pail, R., & Rexer, M. (2013). New ultrahigh-resolution picture of Earth's gravity field. *Geophysical Research Letters*, *40*(16), 4279–4283. https://doi.org/10.1002/grl.50838

Irsyam, M., Widiyantoro, S., Natawidjaya D. H., Meilano, I., Rudyanto, A., Hidayati, S., Triyoso, W., Hanifa, N. R., Djawadi, D., Faizal, L., & Sunarjito. (2017). *Peta sumber dan bahaya gempa Indonesia tahun 2017*. Pusat Penelitian dan Pengembangan Perumahan dan Permukiman, Kementerian Pekerjaan Umum dan Perumahan Rakyat.

Mangga, S. A., Atmawinata, S., Hermanto, B., Setyogroho, B., & Amin, T. C. (1994). *Peta Geologi Lembar Lombok Nusa Tenggara Barat*. Pusat Survey Geologi.

Pratama, I. P. D., Koten, M. C. R., & Negara, P. K. G. A. (2021). Asesmen Katalog Gempabumi di Wilayah PGR III Sebelum dan Setelah Penambahan Sensor Seismik Tahun 2019 Menggunakan Magnitude Completeness. *Buletin GAW Bariri (BGB)*, *2*(1), 37–47. https://doi.org/10.31172/bgb.v2i1.43

Priyono, A., Nugraha, A. D., Muzli, M., Ardianto, A., Aulia, A. N., Prabowo, B. S., Zulfakriza, Z., Rosalia, S., Sasmi, A. T., Afif, H., Sahara, D. P., Widiyantoro, S., Wei, S., Husni, Y. M., & Sarjan, A. F. N. (2021). Seismic Attenuation Tomography from 2018 Lombok Earthquakes, Indonesia. *Frontiers in Earth Science*, *9*(March), 1–16. https://doi.org/10.3389/feart.2021.639692

Pudja, I. P. (2020). Focal validation mechanism for Lombok earthquake with image analysis of satellite radar and crust movement GPS observation. *Sustinere: Journal of Environment and Sustainability*, *4*(1), 24–32. https://doi.org/10.22515/sustinere.jes.v4i1.92

Ramdani, F., Setiani, P., & Setiawati, D. A. (2019). Analysis of sequence earthquake of Lombok Island, Indonesia. *Progress in Disaster Science*, *4*, 100046. https://doi.org/10.1016/j.pdisas.2019.100046

Sasmi, A. T., Nugraha, A. D., Muzli, M., Widiyantoro, S., Syuhada, S., Muttaqy, F., Zulfakriza, Z., Wei, S., Priyono, A., Afif, H., Supendi, P., Husni, Y. M., Prabowo, B. S., & Sarjan, A. F. N. (2023). Shear wave splitting of the 2018 Lombok earthquake aftershock area, Indonesia. *Geoscience Letters*, *10*(1). https://doi.org/10.1186/s40562-022-00258-3

Sarkowi, M. (2010). Identifikasi struktur daerah panasbumi ulubelu berdasarkan analisa data svd anomali bouguer. *J. Sains MIPA, 16*(2), 111-118. Retrieved from https://repository.lppm.unila.ac.id/id/eprint/22328

Soehaimi, A., Sopyan, Y., Ma'mur, & Agustin, F. (2021). *Peta Patahan Aktif Indonesia*. Retrieved from https://geologi.esdm.go.id/geomap/index.php/pages/preview/peta-patahan-aktif-indonesia.

Supendi, P., Nugraha, A. D., Widiyantoro, S., Pesicek, J. D., Thurber, C. H., Abdullah, C. I., Daryono, D., Wiyono, S. H., Shiddiqi, H. A., & Rosalia, S. (2020). Relocated aftershocks and background seismicity in eastern Indonesia shed light on the 2018 Lombok and Palu earthquake sequences. *Geophysical Journal International*, *221*(3), 1845–1855. https://doi.org/10.1093/gji/ggaa118

Telford, W. M., Geldart, L. P., & Sheriff, R. E. (1990). *Applied geophysics*. Cambridge university press.

Zaki Agung, Y., Didit Haryanto, A., Hardiyono, A., Iim Setiawan, D., & Asoka Suleman, W. (2021). High Permeability Zone on Geothermal Manifestations Using Fault Fracture Density in Sembalun Area, Lombok. *Journal of Geological Sciences and Applied Geology* (Vol. 5, Issue 2)

Zhao, S., McClusky, S., Cummins, P. R., & Miller, M. S. (2024). Co-seismic and post-seismic deformation associated with the 2018 Lombok, Indonesia, earthquake sequence, inferred from InSAR and seismic data analysis. *Remote Sensing of Environment*, *304*(February), 114063. https://doi.org/10.1016/j.rse.2024.114063.